J. Fluid Mech. (1999), *vol.* 383, *pp.* 55–73. Printed in the United Kingdom

Prandtl number effects in convective turbulence

By R. VERZICCO[1] AND R. CAMUSSI[2]

[1]Università di Roma 'La Sapienza', Dipartimento di Meccanica e Aeronautica, via Eudossiana 18 00184 Roma, Italia

[2]Università di Roma 'Tre', Dipartimento di Ingegneria Meccanica e Industriale, via della Vasca Navale 79, 00146 Roma, Italia

(Received 3 March 1998 and in revised form 11 September 1998)

The effect of Prandtl number on the dynamics of a convective turbulent flow is studied by numerical experiments. In particular, three series of experiments have been performed; in two of them the Rayleigh number spanned about two decades while the Prandtl number was set equal to 0.022 (mercury) and 0.7 (air). In the third series, in contrast, we fixed the Rayleigh number at 6×10^5 and the Prandtl number was varied from 0.0022 up to 15. The results have shown that, depending on the Prandtl number, there are two distinct flow regimes; in the first ($Pr \lesssim 0.35$) the flow is dominated by the large-scale recirculation cell that is the most important 'engine' for heat transfer. In the second regime, on the other hand, the large-scale flow plays a negligible role in the heat transfer which is mainly transported by the thermal plumes.

For the low-Pr regime a model for the heat transfer is derived and the predictions are in qualitative and quantitative agreement with the results of the numerical simulations and of the experiments. All the hypotheses and the consequences of the model are directly checked and all the findings are consistent with the predictions and with experimental observations performed under similar conditions. Finally, in order to stress the effects of the large-scale flow some counter examples are shown in which the large-scale motion is artificially suppressed.

1. Motivation

The turbulent heat transport between two horizontal surfaces at different temperatures is a model problem that has been considered in countless numerical and experimental studies. The flow dynamics depends essentially on two dimensionless parameters: the Rayleigh (Ra) and Prandtl (Pr) numbers defined as

$$Ra = \frac{g\alpha\Delta d^3}{\nu\kappa} \quad \text{and} \quad Pr = \frac{\nu}{\kappa}\,, \tag{1.1}$$

where Δ, d, α, ν and κ are, respectively, the temperature difference between the surfaces, their separation distance, the thermal expansion coefficient of the fluid, its kinematic viscosity and its thermal diffusivity.

Equation (1.1) shows that the Rayleigh number depends on the fluid type but also on the cell geometry and experimental conditions; in contrast, Pr is essentially fixed once the fluid is chosen. From an experimental point of view it is quite easy to vary the Rayleigh number over several decades by changing Δ and d while the Prandtl number can take only a limited number of discrete values obtained using different fluids.

Most common fluids have values of Pr in the range 1–10 or much bigger ($Pr \simeq 0.7$

for air and gaseous helium, $Pr \simeq 7$ in water and $Pr = O(10^3)$ for silicon oils) and these have been extensively studied in the literature owing to their relevance in theoretical and practical applications. Flows with Prandtl number much smaller than unity are very important as well (in the Earth's liquid core convection, crystal growth in semiconductors, melting processes etc.) and they are obtained using liquid metals. Mercury is a commonly used fluid since it is liquid at ambient temperature; in contrast, for sodium a mean temperature above 373 K is needed. The use of different liquid metals poses serious practical problems such as poisoning, over-expensive materials or very high mean temperatures. This implies that the experimental analysis of the low Pr region is limited to essentially two fluids in a flow regime where a strong dependence of heat transfer on Prandtl is observed.

Numerical simulations, on the other hand, suffer from the inherent limitations of spatial resolution but a continuous variation of the Prandtl number within the desired range can be performed without problems. This suggests that, for low Prandtl number turbulent convection, numerical and laboratory experiments could be used as complementary tools in order to obtain a deeper knowledge of the flow dynamics. This consideration forms the main motivation for the present study.

In this paper we consider the turbulent thermal convection evolving in a cylindrical cell of unity aspect ratio (cell diameter/height) for several values of the Rayleigh and Prandtl numbers. This configuration has been already considered by Takeshita *et al.* (1996) in mercury, by Cioni, Ciliberto & Sommeria (1997) in mercury and water and by Castaing *et al.* (1989) in gaseous helium. The availability of these experiments performed in identical conditions made possible a comparison of the results and allowed the extension of the conclusions to a wider range of parameters. We have performed three series of numerical simulations in which we have filled the gaps in the experimental data at $Pr \simeq 0.022$ (mercury) for $Ra \leqslant 10^6$, at $Pr \simeq 0.7$ (air and gaseous helium) for $Ra \leqslant 2 \times 10^7$ and at fixed Ra for $0.022 \leqslant Pr \leqslant 15$. From the integrated analysis of the data from simulations and experiments a clearer picture of the flow dynamics has emerged. In particular a threshold value of the Prandtl number ($Pr_t \approx 0.35$) has been found that separates distinct flow regimes. For Prandtl number above this threshold the heat transport is essentially due to the thermal plumes, consistent with the scenario proposed by Castaing *et al.* (1989). In contrast, below Pr_t thermal plumes are not generated and the heat is efficiently transported by the large-scale flow. This flow structure is the basis of the 'flywheel' model by Jones, Moore & Weiss (1976) and later by Busse & Clever (1981) that in the present paper has been validated and extended. This model is in quantitative agreement with experiments and simulations and predicts the correct Rayleigh and Prandtl number dependence of the Nusselt number for $Pr < Pr_t$.

2. Problem description and numerical set-up

In this paper we study the flow generated by thermal convection processes in a set-up which is identical to the experimental set-up of Cioni *et al.* (1997). Details and sketches are in Verzicco & Camussi (1997) and Camussi & Verzicco (1998); here only a short description is given. The fluid is confined in a cylindrical cell; let D be the diameter of the cell and d the distance between the lower hot and upper cold horizontal plates. The aspect ratio of the cell $\Gamma = D/d$ is 1 for all the simulations. The gravity vector points downwards and is orthogonal to the upper and lower plates which are maintained at constant temperature. The lateral wall of the cell is adiabatic with the condition of zero heat flux. All the boundaries are no-slip.

The three-dimensional time-dependent Navier–Stokes equations with the Boussinesq approximation for an incompressible viscous fluid have been integrated numerically. The equations have been made non-dimensional using the 'free-fall' velocity $\mathscr{U} = (g\alpha\Delta d)^{1/2}$, the distance d between the horizontal plates and their temperature difference Δ giving

$$\frac{\partial \boldsymbol{u}}{\partial t} + \boldsymbol{u}\cdot\nabla\boldsymbol{u} = -\nabla p + Q\hat{\boldsymbol{x}} + \left(\frac{Pr}{Ra}\right)^{1/2}\nabla^2\boldsymbol{u}, \tag{2.1}$$

$$\nabla\cdot\boldsymbol{u} = 0, \tag{2.2}$$

$$\frac{\partial Q}{\partial t} + \boldsymbol{u}\cdot\nabla Q = \frac{1}{(PrRa)^{1/2}}\nabla^2 Q, \tag{2.3}$$

where $\boldsymbol{u}$ is the velocity vector, $\hat{\boldsymbol{x}}$ the gravity unity vector and p the pressure. Q denotes the non-dimensional temperature defined as $Q = (T - T_c)/\Delta$ so that $0 \leqslant Q \leqslant 1$; T_c is the temperature of the upper cold plate.

The equations, in a cylindrical coordinate system in terms of primitive variables (velocity and pressure), have been discretized using second-order-accurate finite-difference approximations in space and in time. The solution procedure is essentially that of Verzicco & Orlandi (1996) with the modifications described in Verzicco & Camussi (1997). Here it is enough to note that the system of discretized equations is solved by a fractional-step method and the advancement in time is performed by a third-order Runge–Kutta scheme.

The grid independence of the results has been checked for every simulation. In particular we have used the criterion given by Grötzbach (1983) that the mean grid size $\delta = (r\Delta\theta\Delta r\Delta x)^{1/3}$ is smaller than the smaller of the Kolmogorov scale and the diffusive temperature scale. This constraint gives for $Pr < 1$, $\delta \leqslant \pi(Pr^2/RaNu)^{1/4}$, while for $Pr \geqslant 1$, $\delta \leqslant \pi(1/Pr^2RaNu)^{1/4}$. Another condition to be satisfied is that the boundary layers are properly spatially resolved. This implies that within the thinner of the thermal boundary layer ($\delta_T/d \approx 1/2Nu$) and the viscous boundary layer ($\delta_v \sim \delta_T Pr$) there are at least 3–5 grid points (Grötzbach 1983). The satisfaction of all these constraints implied that grids ranging from $33\times33\times65$ up to $85\times97\times193$ in the radial, azimuthal and vertical directions (r, θ and x), respectively, had to be used. The upper limit was fixed by the power of the computer available and this, in turn, posed a limitation on the range of parameters that could be explored. In particular at $Pr = 0.022$ (mercury) we could simulate Rayleigh numbers up to $Ra = 10^6$ while at $Pr = 0.7$ (air) the maximum was $Ra = 2\times10^7$. As a further check we have performed a grid independence test for the most critical cases ($Pr = 0.022$, $Ra = 10^6$ and $Pr = 0.7$ and $Ra = 2\times10^7$). According to Grötzbach (1983) the Nusselt number is the quantity most sensitive to the spatial resolution and when the above simulations were repeated using a grid $65\times65\times129$ only negligible differences with the finest grid (the two values of the Nusselt number were within the error bars) were observed.

Concerning the initial conditions, one simulation was restarted from the field obtained by an axisymmetric case with small-amplitude random noise superimposed on the temperature. The field was then evolved until a statistical steady state, observed in the energy modes, was attained (see figure 2 of the paper by Verzicco & Camussi 1997). The simulation was then run for at least 30 large-eddy-turnover times (defined as $\mathscr{T} = \pi d/\mathscr{U}$) to accumulate statistics and fields. This procedure, however, was time consuming, and therefore it was followed only for the run at $Ra = 6\times10^5$ and $Pr = 0.022$. For the other cases, the runs were initiated by a fully developed field at

the closest Ra and Pr with a sudden change in the parameters to the desired value. Of course in this case the flow also underwent an adjustment but it was only 1–2 large-eddy-turnover times long. Once the flow adjusted to the new equilibrium state the simulation was continued for 30–50 large-eddy-turnover times and the results then analysed. The need to run each case for such a long time was due to convergence of the statistical quantities when the flow was turbulent. In particular, every simulation was run until the values of the Nusselt number averaged over a time $\bar{t}$ and of its r.m.s. did not change when averaged over a time $\bar{t} - 10\mathscr{T}$. Further details are given in Verzicco & Camussi (1997) and Camussi & Verzicco (1998).

3. Results

3.1. *Fundamentals*

The Nusselt number $Nu = Hd/\kappa\Delta$ is defined as the quantity of heat per unit surface H transferred between the hot and cold plates, normalized with the conductive heat $\kappa\Delta/d$ that is the heat transferred in the absence of convective motion. In order to clarify the Nu dependence on the flow parameters we have performed three series of numerical simulations; in two of them 'low' and 'high' Prandtl numbers ($Pr = 0.022$ and $Pr = 0.7$) were used, with the Rayleigh number varied in such a way as to obtain a sufficiently long power law range of the Nu vs. Ra relation (the value $Pr = 0.7$ cannot be considered 'high' but rather moderate; however, in the following, it will be shown that the fluid dynamics do not change when a threshold value for Pr is exceeded and $Pr = 0.7$ is already beyond such threshold). In the third series of simulations, the Rayleigh number was fixed at $Ra \simeq 6 \times 10^5$, while the Prandtl number covered the range $2.2 \times 10^{-3} \leqslant Pr \leqslant 15$. The results of the simulations are summarized in figure 1 where some additional experimental and numerical data are also reported for comparison. It is immediately evident that there are two flow regimes; in the first (for $Pr \lesssim 0.35$) the Nusselt number increases with Pr while in the second the Nusselt number is independent of Pr (see figure 1*b*). This independence can be also appreciated from figure 1(*a*) where results at $Pr = 0.35$, $Pr = 0.7$ and $Pr = 7$ show indistinguishable behaviour.

Another important feature is the exponent β of the relation $Nu \sim Ra^{\beta}$ that in the low Pr case ($\beta = 0.25 \pm 0.004 \simeq 1/4$) is smaller than in the high Pr case ($\beta = 0.285 \pm 0.004 \simeq 2/7$). This difference might appear negligible; however, in the range of Ra of common applications ($Ra \approx O(10^7$–$10^{10})$) such a small deviation could imply errors in the predicted heat transfer of more than 100%.

The high Pr regime has already been widely investigated numerically and experimentally and many characteristics of the flow field have been understood from flow visualizations. Starting from assumptions based on experimental evidence the exponent $\beta = 2/7$ has been given several theoretical explanations. Shraiman & Siggia (1990) found this exponent by considering the structure of the mean flow. Their fundamental hypotheses were that (i) the thermal boundary layer is contained within the viscous velocity sublayer; (ii) the persistent mean flow close to the horizontal plates generates a velocity parallel to the plates that increases with the distance ($U \sim x$) thus yielding a linear profile. These hypotheses led Shraiman & Siggia to the scaling law $Nu \sim Ra^{2/7}$. In some recent experiments, however, Ciliberto, Cioni & Laroche (1996) have found that the Nusselt number in water does not change when screens are placed inside the domain so that the recirculation cell is destroyed. This would suggest that in the high Pr regime the large-scale motion is ineffective in the heat

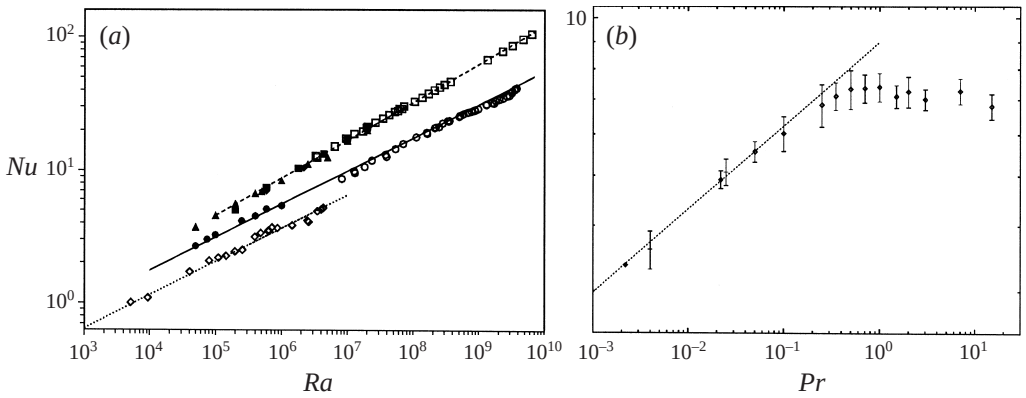

FIGURE 1. (*a*) Nu vs. Ra relation for different Pr: •, present numerical results at $Pr = 0.022$; ▪, present numerical results at $Pr = 0.7$; ◆, present numerical results at $Pr = 0.35$; ▲, numerical results by Kerr (1996) at $Pr = 0.7$; ○, experimental results by Cioni *et al.* (1997) at $Pr = 0.025$; □ , experimental results by Cioni *et al.* (1997) and by Chillá *et al.* (1993) at $Pr = 4.0$; ◇, experimental results by Horanyi *et al.* (1997) at $Pr = 0.005$; – – – –, fit $Nu \sim Ra^{0.285}$; ———, fit $Nu \sim Ra^{0.25}$; ·····, fit $Nu \sim Ra^{0.25}$. (*b*) Nu vs. Pr relation at $Ra = 6 \times 10^5$: – – – –, fit $Nu \sim Pr^{0.14}$: ◇, present numerical results; -, experimental results from Horanyi *et al.* (1997) and Rossby (1969) for sodium and mercury, respectively (the value of Rossby has been corrected to account for the different aspect ratio of his cell according to Belmonte *et al.* 1994).

transfer which is dominated instead by the motion of the thermal plumes. This is the main assumption made by Castaing *et al.* (1989) who found the $Nu \sim Ra^{2/7}$ law assuming that the main mechanism of heat transfer is due to thermal plumes that move in the bulk of the flow with constant velocity. This conjecture has also been confirmed by the experiments in helium and water of Belmonte, Tilgner & Libchaber (1994) who, from a local relation between heat flux and shear at the plates, found the large-scale circulation to be too weak to balance the observed heat flux. They note that thermal plumes coexist with the large-scale circulation and they must be responsible for most of the heat flux.

The results for low Pr show a substantial disagreement with both theories as confirmed by figure 1(*a*). The reason for this disagreement is the structure of the flow that, in this Pr regime, does not satisfy either the thermal plume scenario of Castaing *et al.* (1989) or the flow structure proposed by Shraiman & Siggia (1990). It is evident from the snapshot of figure 2(*a*) that the diffusive nature of the temperature field does not allow the formation of plumes. In addition, given $Pr \ll 1$, we expect the viscous boundary layer to be contained within the thermal boundary layer and not vice versa.

The presence of a distinct flow regime with different flow features is a fundamental point for low-Pr thermal convection and it deserves careful investigation by visualization and direct measurement. Unfortunately these checks are very difficult to perform experimentally since this regime pertains to liquid metals. In these fluids flow visualization is impossible and many measurements become problematic. On the other hand the numerical simulations are also difficult because low Pr yields a large Reynolds number at moderate Ra. However, recent papers by Verzicco & Camussi (1997) and Camussi & Verzicco (1998) have shown that in mercury, $Pr \approx 0.022$, the flow features observed in the range of $Ra = 5 \times 10^4 - 10^6$ are similar and consistent with the experimental results at higher Ra ($O(10^7$–$10^{11})$) found by Cioni *et al.* (1997) and Takeshita *et al.* (1996). This implies that the flow structure can be investigated

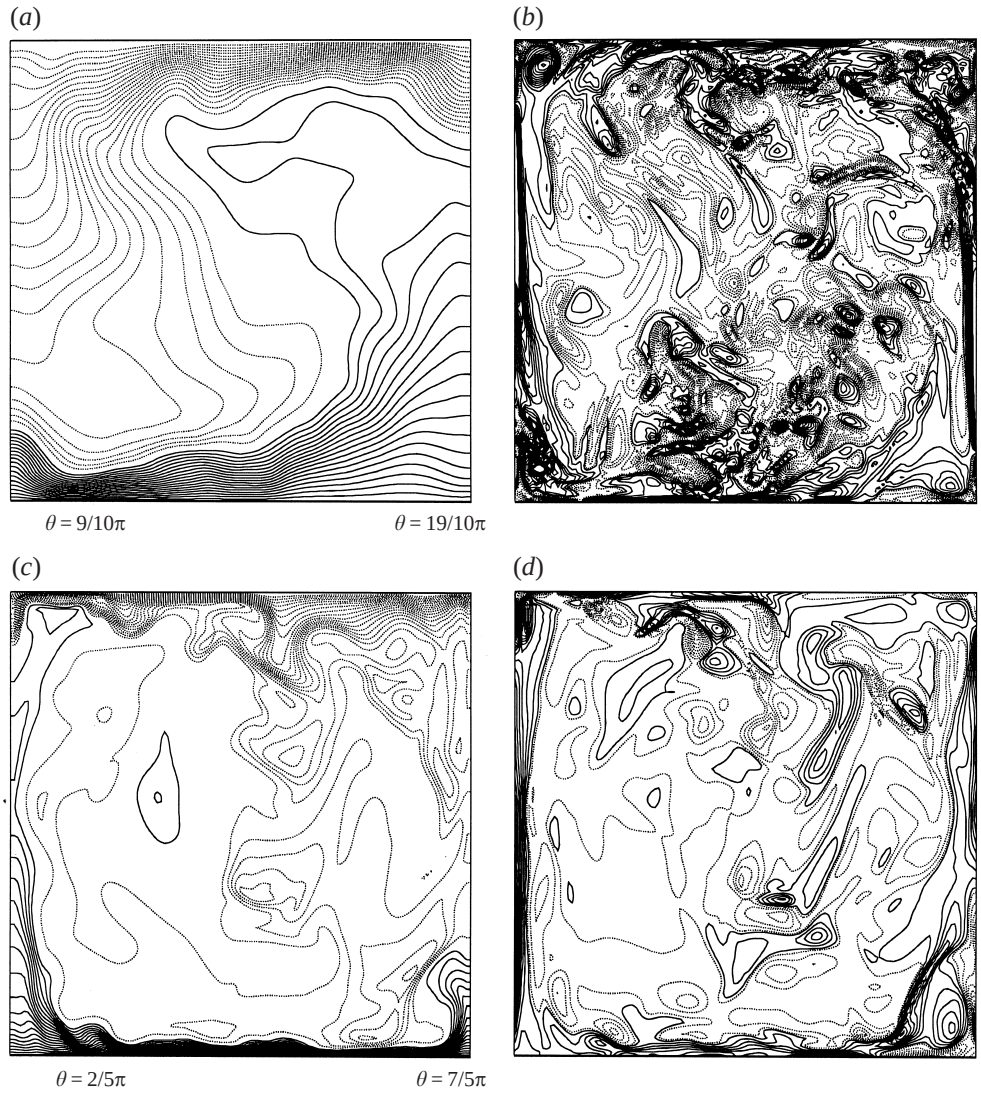

FIGURE 2. Snapshots of vertical cross-sections at $Pr = 0.022$ and $Ra = 10^6$ (a, b) and at $Pr = 0.7$ and $Ra = 2 \times 10^7$ (c, d). Left, temperature contour plots: ———, $0.5 \leqslant Q \leqslant 1$; ·····, $0 \leqslant Q < 0.5$ ($\Delta Q = 0.05$). Right, azimuthal vorticity: ———, clockwise; ·····, counter-clockwise rotation ($\Delta\omega = 2.0$).

in detail with the convenience of numerical simulations and, once the main features have been understood, new assumptions can be made about the flow dynamics. Of course it must be verified, *a posteriori*, that both assumptions and conclusions based on the limited Ra range afforded by numerical simulations are in agreement with the available experimental results for higher Ra.

In figure 2 snapshots of vertical sections of azimuthal vorticity and temperature are shown for two cases at low and high Pr. As we expect from the above discussions, the thermal boundary layer in the low Pr case is much thicker than in the other case while the opposite happens for the velocity boundary layer (see also figure 4 and related discussion). We see that while the thermal boundary layers for high Pr are

dominated by plumes shed at random positions from the horizontal plates (figure 2*c*) the low Pr temperature field is substantially different (figure 2*a*). In particular the large thermal diffusivity prevents thermal plumes from being generated and the persistent recirculation cell induces a rising hot current on the right and a sinking cold current on the left that dominate the field. The same conclusions about the absence of plumes and the mean flow were reached by Takeshita *et al.* (1996) from experiments in mercury in the range of Rayleigh number 10^6–10^8. Previous numerical simulations (Verzicco & Camussi 1997) have shown that this flow structure is very robust since it preserves similar features from the onset of convection up to the fully turbulent regime. In addition, Cioni *et al.* (1997) have given indirect proof that the same flow is observed even for Rayleigh numbers up to 10^{10}. This suggests that a model for the heat transfer can be proposed by considering a mean flow structure like the one described above.

3.2. *Theory*

There is numerical and experimental evidence that the vertical temperature difference Δ between hot and cold plates is mostly sustained within the thermal boundary layers, while in the bulk of the flow the temperature is nearly constant (figure 3 *a*, *b*). Denoting by δ_T the thickness of the thermal boundary layer, we have $H \approx \frac{1}{2}k\Delta/\delta_T$, the factor $\frac{1}{2}$ coming from the fact that only half of the temperature difference is present in each boundary layer. From these definitions it follows that $Nu \approx d/(2\delta_T)$ indicating that the Nusselt number is related to the inverse of the non-dimensional thermal boundary layer thickness. Now we focus on the temperature equation inside the thermal boundary layer by considering the structure of the mean flow. The strong recirculation cell induces a persistent 'wind' which sweeps the plates with a velocity (U) in the horizontal direction (y) and generates a boundary layer much thinner than the thermal boundary layer. Another effect of the cell is the generation of cold descending and hot rising currents that in turn generate a horizontal temperature difference Δ_h. The different thicknesses of the boundary layers allow us to assume that inside the thermal boundary layer the velocity is approximately constant and mainly horizontal so that when the temperature equation is averaged in time the nonlinear terms reduce to $U\partial T/\partial y$. For the viscous terms we can use a boundary layer assumption in which all the gradients other than that normal to the wall are neglected. In the fully turbulent regime we expect statistical steadiness of the flow and therefore the temperature equation reads

$$U\frac{\partial T}{\partial y} \approx \kappa\frac{\partial^2 T}{\partial x^2}, \tag{3.1}$$

where time averaging of each term is implied. At this point we must relate U and $\partial T/\partial y$ to the flow parameters so that some information on the Nusselt number can be obtained. We assume, then, that the velocity U is proportional to the free-fall velocity $U \approx A\mathscr{U}$ and that the horizontal temperature difference Δ_h is proportional to the total temperature difference $\Delta_h \approx B\Delta$. Finally, in a recirculation cell of aspect ratio 1 we have $\partial T/\partial y \approx \Delta_h/d$ and the above equation becomes

$$A(g\alpha\Delta dB)^{1/2}\frac{\Delta}{d} \approx \frac{\kappa\Delta}{2\delta_T^2} \qquad \Rightarrow \qquad Nu \approx \left(\frac{AB}{2}\right)^{1/2}(RaPr)^{1/4}. \tag{3.2a,b}$$

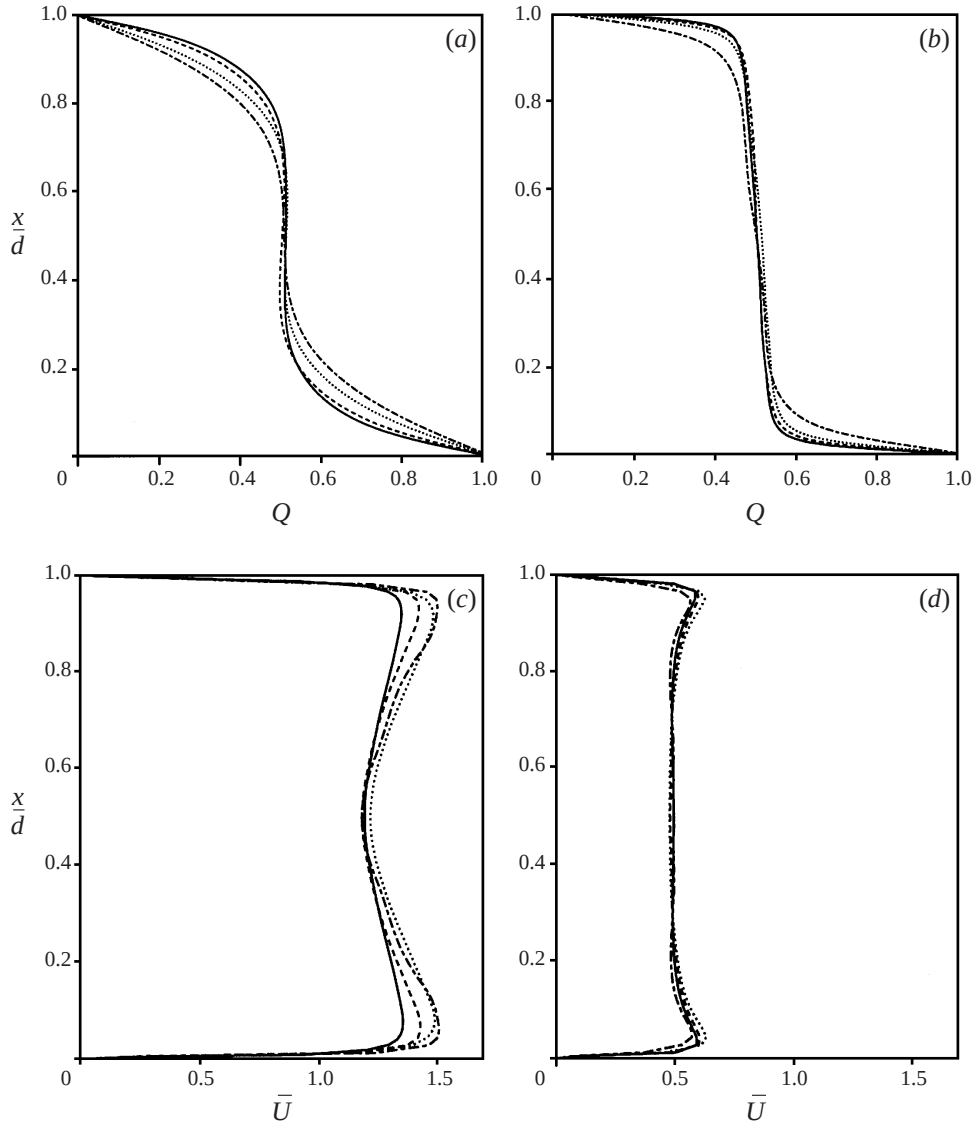

FIGURE 3. Averaged vertical temperature profiles: (*a*) $Pr = 0.022$: ———, $Ra = 10^6$; – – – –, $Ra = 6 \times 10^5$; ·····, $Ra = 2.5 \times 10^5$; — – —, $Ra = 5 \times 10^4$. (*b*) $Pr = 0.7$, the same sequence as (*a*) for $Ra = 2 \times 10^7$, $Ra = 10^7$, $Ra = 4.5 \times 10^6$ and $Ra = 1.8 \times 10^6$. Averaged velocity profiles: (*c*) $Pr = 0.022$: ———, $Ra = 10^6$; – – – –, $Ra = 6 \times 10^5$; ·····, $Ra = 2.5 \times 10^5$; — – —, $Ra = 5 \times 10^4$. (*d*) $Pr = 0.7$, the same sequence as (*c*) for $Ra = 2 \times 10^7$, $Ra = 10^7$, $Ra = 4.5 \times 10^6$ and $Ra = 1.8 \times 10^6$.

The factors A and B have been left unspecified for the moment to stress that in principle both of them could depend on Ra and Pr in a complicated way† thus

† It should be stressed that in order to hold the proportionality between U and Δ_c and the free-fall velocity and total temperature difference respectively, A and B can depend only on Pr. In fact, Ra contains Δ and the dependence of A and B on Ra would change the proportionality. Nevertheless, at the moment we prefer to leave this possibility open to point out that $U \approx A\mathscr{U}$ and $\Delta_c \approx B\Delta$ are only assumptions that need to be proved by direct evaluation. These checks are performed in the next section.

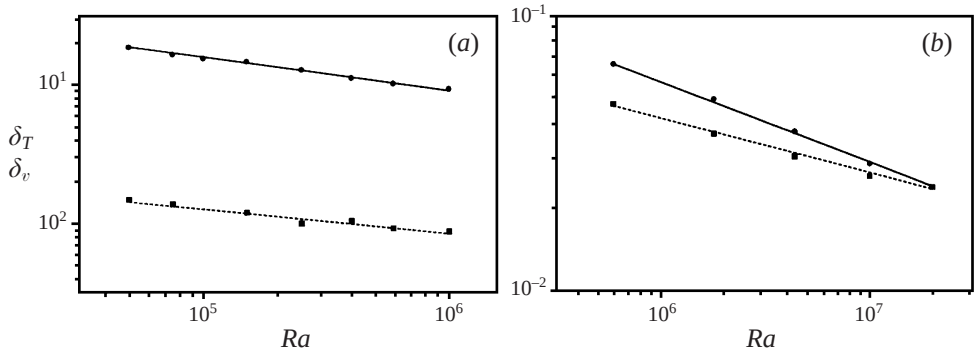

FIGURE 4. (*a*) Viscous (▪) and thermal (•) boundary layer thicknesses vs. Ra at $Pr = 0.022$: ———, $\delta_T = 2.8Ra^{-0.25}$; – – – –, $\delta_v = 0.1Ra^{-0.18}$ fits. (*b*) The same as (*a*) at $Pr = 0.7$: ———, $\delta_T = 3.1Ra^{-0.29}$; – – – –, $\delta_v = 0.95Ra^{-0.23}$ fits.

making the prediction (3.2) useless. However, while verifying all the hypotheses leading to the above relation, we will see that this is not the case and only the coefficient A has a dependence on Pr; when this dependence is accounted for, the relation (3.2) predicts well the Ra and Pr dependence of the Nu number in the low-Pr regime.

A similar model was derived by Jones *et al.* (1976) who, speculating about the nature of convection between free boundaries, obtained $Nu \sim (RaPr)^{1/4}$. The assumption of a free-slip wall is equivalent to positions in our flow where the viscous boundary layer is supposed to be much thinner than the thermal one so that the latter is swept by a constant velocity. Busse & Clever (1981) by an approximate solution of two-dimensional steady convection in the limit of low Pr obtained $Nu \sim Ra^{1/4}$ without any Pr dependence. In particular, starting from the arguments of Jones *et al.* (1976) they assumed that the convection roll exhibits a 'flywheel' character thus producing an inertial convection. In our model there is a very similar assumption since, even if the large scale is neither steady nor two-dimensional, we resort to some induced effects, like the permanent horizontal temperature difference or the horizontal velocity sweeping the thermal boundary layers, that imply a 'flywheel'-like large-scale flow at least in the statistical sense. In conclusion this model is essentially the same as that proposed by Jones *et al.* (1976); however, we included the ingredients to obtain the correct Pr dependence and to extend the model to the turbulent regime. In addition, using the results of the numerical simulation and the available experimental data we could check all the hypotheses and the validity limits.

The first hypothesis to be verified for (3.1) to be valid is that the viscous boundary layer is always contained within the thermal boundary layer and that no crossing occurs. In figure 4 we report the results obtained by direct estimation of the boundary layer thicknesses from the temperature- and velocity-averaged profiles of figure 3. As previously done in several papers (e.g. Takeshita *et al.* 1996; Belmonte *et al.* 1994), all the thicknesses have been measured from the position at which the extrapolation of the linear portion of the profile equals the central mean value of the temperature and the maximum horizontal velocity for δ_T and δ_v, respectively. It should be noticed that the present definition of δ_v is different from the boundary layer thickness λ_v defined by Shraiman & Siggia (1990) and discussed by Kerr (1996). However, it can be shown that their relation is simply given by $\lambda_v = 2\nu^{1/2}\delta_v^{1/2}/\overline{U}^{1/2}$, $\overline{U}$ being the magnitude of the maximum horizontal velocity. Therefore the transformation from one definition to the other is very easy once λ_v or δ_v are known. From figure 4, it is

evident that in the low Pr regime the first hypothesis in (3.1) is always verified and even though the thermal boundary layer thickness decreases faster than the viscous one, if a crossing occurred it would be only for $Ra \approx O(10^{20})$ where a different flow regime ($Nu \sim Ra^{1/2}$) is known to apply†. The situation is quite different for $Pr = 0.7$ where the boundary layers are always of comparable thickness and a crossing has occured at $Ra = 2 \times 10^7$. This might only be a fortuitous coincidence; however, B. Castaing (personal communication) states that in a cylindrical cell of unity aspect ratio in gaseous helium ($Pr \simeq 0.7$) starting from the value of $Ra = 2 \times 10^7$ he observed all the turbulent quantities to follow a well defined power law behaviour with Ra.

These results agree with the experiments performed in similar conditions. In the high Pr regime, for example, we have found for the non-dimensional thermal boundary layer thickness $\delta_T/d = 3.1Ra^{-0.29}$ while Belmonte *et al.* (1994) and Xin, Xia & Tong (1996) found respectively $\delta_T/d = 3.14Ra^{-0.29}$ and $\delta_T/d = 3.54Ra^{-0.29}$ even though the former used a cubic cell and the latter did the experiment in water. For the viscous boundary layer we obtained $\delta_v/d = 0.95Ra^{-0.23}$ while Xin *et al.* (1996) found $\delta_v/d = 0.51Ra^{-0.16}$. In this case the results are more scattered; however, this might be due to the difficulty of velocity measurements in thermal convection flows. Similar results were obtained by Kerr (1996) who observed at $Pr = 0.7$ that δ_T/d decreases with Ra faster than δ_v/d. We wish to stress that the present results agree also with the definition of Shraiman & Siggia (1990) since we have $\delta_v \sim Ra^{-0.23}$ and $\overline{U} \sim Ra^{0.5}$ (see the next section) which give $\lambda_v \sim Ra^{-0.38}$; this value is close to their theoretical prediction $\lambda_v \sim Ra^{-3/7}$.

In the low Pr regime Naert, Segawa & Sano (1997) obtained for both boundary layers a thickness decrease as $Ra^{-0.2}$. They used a fitting of the profiles with the function $\tanh(x/\delta)$ and estimated the boundary layer thicknesses with δ; however, when the present criterion was used they found $\delta_T/d \sim Ra^{-0.25}$ (A. Naert, personal communication). These results agree quite well with ours of figure 4(a) being $\delta_T/d \sim Ra^{-0.25}$ and $\delta_v/d \sim Ra^{-0.18}$.

In conclusion, from all the available data, we can say that even though there is some scatter possibly due to thickness definitions, measurement uncertainties and different experimental set-ups, in the low Pr regime the condition $\delta_v \ll \delta_T$ is always satisfied while in the high Pr regime the thicknesses cross for some value of Ra and eventually the condition $\delta_T \ll \delta_v$ applies.

Briefly, we note that the exponents γ of our fits $\delta_T \sim Nu^{\gamma}$ are exactly the opposite of those of $Nu \sim Ra^{\beta}$ thus confirming the consistency of the results with $Nu \sim \delta_T^{-1}$.

3.3. *Nusselt number dependence on Rayleigh number*

In the previous section we have derived the relation (3.1) and we have shown its validity in the low Pr regime. In this section we discuss and validate the hypotheses leading from (3.1) to (3.2) showing some comparisons with other experimental and numerical results.

A first important point to be checked is the Ra dependence of the horizontal velocity U sweeping the plates. Given the incompressibility of the flow and the shape

† According to Kraichnan (1962) there is a threshold value for the Rayleigh number after which the heat is transferred much more efficiently ($Nu \sim Ra^{1/2}$). This range is known as the asymptotic limit and Cioni *et al.* (1997) have found that for $Ra \approx O(10^9$–$10^{10})$ a transition might indeed be present for the mercury. In contrast Castaing *et al.* (1989) in gaseous helium increased the Ra up to 10^{13} without measuring any change in the slope of the Nu vs. Ra relation. Although some transition is expected in the limit of increasing Ra this is a controversial point and some *ad hoc* experimental work is needed before drawing any conclusion.

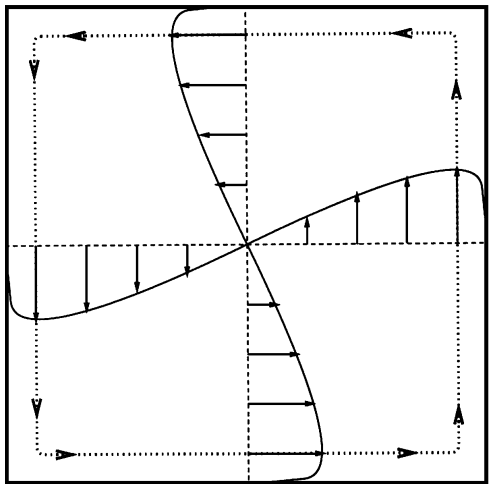

FIGURE 5. Schematic of the velocity induced by the cell.

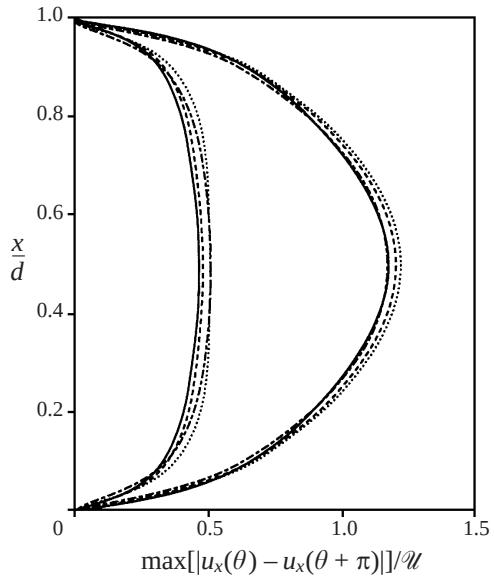

FIGURE 6. Vertical profiles of vertical velocity difference $\max[|u_x(\theta)-u_x(\theta+\pi)|]$; the flatter curves are at $Pr = 0.7$: ———, $Ra = 2 \times 10^7$; – – – –, $Ra = 10^7$; ·····, $Ra = 4.5 \times 10^6$; — – —, $Ra = 1.8 \times 10^6$. The peaky curves are at $Pr = 0.022$: ———, $Ra = 10^6$; – – – –, $Ra = 6 \times 10^5$; ·····, $Ra = 4 \times 10^5$; — – —, $Ra = 2.5 \times 10^5$.

of the recirculation cell, the maximum horizontal difference of the vertical velocity evaluated at the mid-plane $x/d = 0.5$ must equal the maximum vertical difference of the horizontal velocity at the axis, which is twice the velocity U (figure 5). These profiles for several Ra are reported in figure 6 showing that the assumption $U \approx A\mathscr{U}$ is valid and a dependence of A on Ra can be ruled out. The same happens for $Pr = 0.7$ even though the velocity magnitude is more than twice as small.

Similarly to the velocity, the Rayleigh number dependence of the horizontal temperature difference has also to be analysed; this temperature difference Δ_h is induced by the large-scale motion and the profiles are shown in figure 7(*a*). In this case the

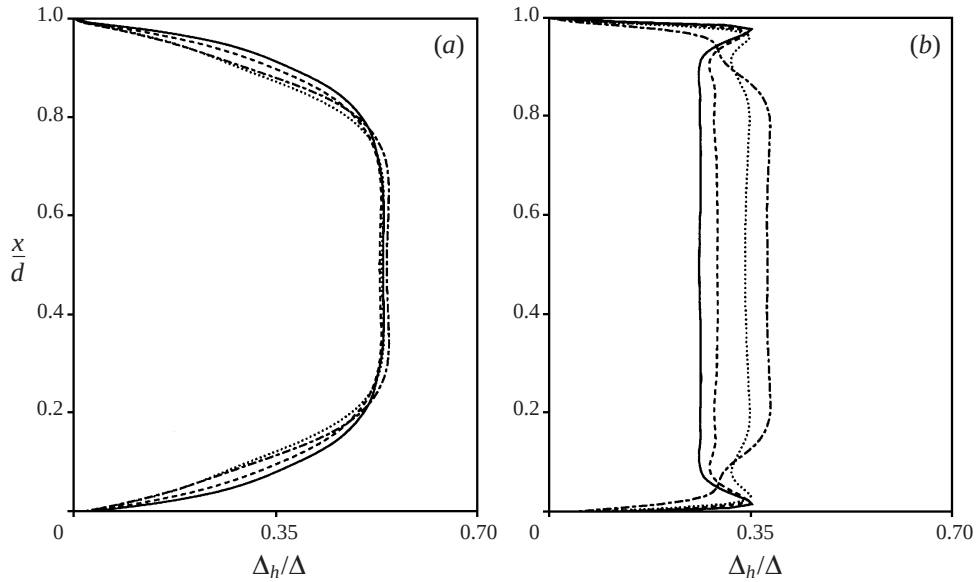

FIGURE 7. The same as figure 6, but for the maximum horizontal temperature difference. (*a*) $Pr = 0.022$, (*b*) $Pr = 0.7$.

assumption $\Delta_h \approx B\Delta$ is also verified and this excludes, in the low Pr regime, the dependence of B on Ra. This result is in apparent disagreement with the experimental findings of Cioni *et al.* (1997) who presented an indirect estimate of Δ_h. Nevertheless, they directly measured only the maximum temperature difference on the plates Δ_p, which was indeed found independent of Ra. Afterwards, using a simplified model, a number of assumptions were made to relate Δ_p to Δ_h and this could be the reason for the weak dependence they found of Δ_h on Ra. Nevertheless, they pointed out that this conclusion must be taken with caution since their measurement of Δ_h is indirect. In figure 7(*b*) we show the same profiles as for figure 7(*a*) but for $Pr = 0.7$. As for the horizontal velocity, the temperature difference is also weaker than in the low Pr case but now it decreases as Ra increases. This is due to the thermal plumes that for increasing Ra detach more frequently and at random positions. This effect, when averaged in time, tends to cancel any horizontal temperature inhomogeneity thus yielding a decreasing Δ_h for increasing Ra.

Coming back to the low Pr regime we have seen that the factors A and B are both independent of Ra; therefore when Pr is fixed (3.2) yields $Nu \sim Ra^{1/4}$ which agrees with the results found for mercury (Verzicco & Camussi 1997; Cioni *et al.* 1997; Rossby 1969; Naert *et al.* 1997) and for sodium (Horanyi, Krebs & Müller 1997). In addition, from figure 6 and figure 7(*a*) we can compute the numerical values of A and B at $Pr = 0.022$ that when inserted into (3.2*b*) give $Nu \approx 0.16Ra^{1/4}$, which is in surprisingly good agreement with the fit given in figure 1(*a*) for the mercury. The fact that not only the exponent but also the numerical factor in the Nu vs. Ra relation is very well predicted indicates that the essential features of the heat transfer mechanism are captured by the present model in the low Pr regime.

Before concluding this section, we wish to point out another result implied by the present model. The direct dependence of the velocity scale U on the free-fall velocity $\mathscr{U}$ implies that the Reynolds number increases with Rayleigh number according to $Re \sim Ra^{1/2}$. This results is confirmed by figure 8(*a*) and, given the good collapse of the

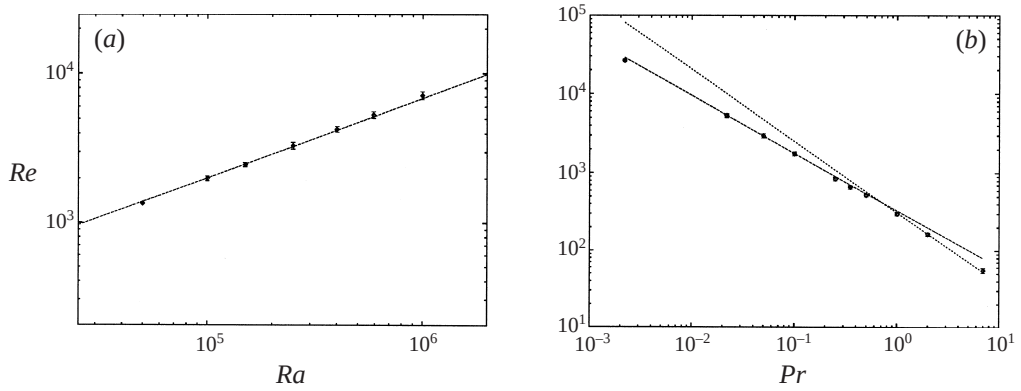

FIGURE 8. (*a*) Reynolds vs. Rayleigh numbers curve at $Pr = 0.022$: symbols, numerical data; ———, $Re \sim Ra^{0.53}$ fit. (*b*) Reynolds vs. Prandtl number curve at $Ra = 6 \times 10^5$: symbols, numerical data; ———, $Re \sim Pr^{-0.73}$ fit; – – – –, $Re \sim Pr^{-0.94}$ fit.

velocity profiles of figure 6, we have the same behaviour in the high Pr regime. The same result was obtained by Tilgner (1996) even though he considered self-gravitating concentric spheres, a configuration which does not allow a straightforward comparison with the present results.

From the experimental side, due to technical difficulties in the velocity measurements, the velocity behaviour has often been conjectured from the peak frequency (f_p) of the temperature spectra. Indeed, if the peak frequency is the signature of the large-scale convective cell its inverse gives the large-eddy turnover time from which information on the velocity is obtained. Castaing *et al.* (1989) and Ciliberto *et al.* (1996) both found $f_p \sim Ra^{0.49}$ in gaseous helium and water respectively while Xin *et al.* (1996) using a novel light scattering technique were able to measure velocities in water directly obtaining $U \sim Ra^{0.5}$. These results imply in the high Pr regime the scaling $Re \sim Ra^{0.5}$ which has been confirmed by several numerical and experimental studies. In contrast, in mercury $f_p \sim Ra^{0.428\pm0.005}$ has been reported by Cioni *et al.* (1997), Camussi & Verzicco (1998) and $f_p \sim Ra^{0.44\pm0.02}$ and $f_p \sim Ra^{0.46\pm0.02}$ have been found by Naert *et al.* (1997) and Takeshita *et al.* (1996). From these results it has been conjectured that the Reynolds number has a similar dependence on the Rayleigh number, which is against the hypothesis for the present heat transfer model. However direct computations of the velocities (present results and Tilgner 1996) have shown that the condition $Re \sim Ra^{0.5}$ indeed holds at low Pr. This means that, at least in the low Pr regime, the correspondence between f_p and U is not direct and all the consequences deriving from this assumption should be considered with care. In particular, using the data of the present simulations at $Pr = 0.022$ and the data for f_p from Camussi & Verzicco (1998) we have found the relation $U/(d f_p) = 1.345 Ra^{0.1}$ which is not a constant in Ra. We wish to stress however, that this relation has been obtained only from a limited range of Ra obtainable by numerical simulation and experimentally measured velocities at higher Ra would help to validate the above expression.

3.4. *Nusselt number dependence on Prandtl number*

The analysis of the Prandtl number dependence of the flow relies on fewer experimental data than the previous section for the reasons already discussed in the Introduction. Furthermore there are few numerical simulations for high and low values of Pr and

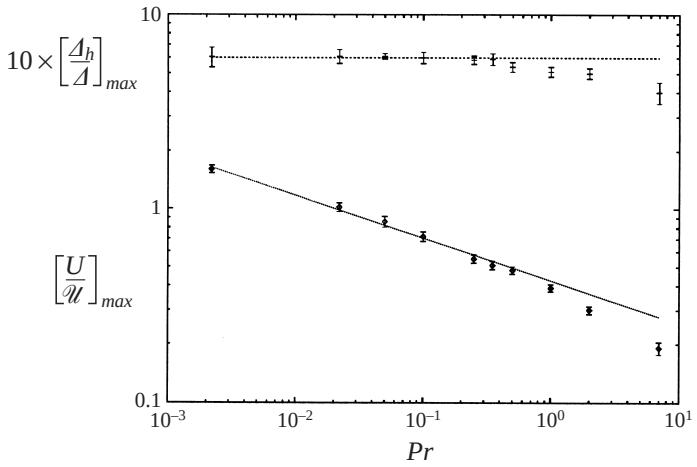

FIGURE 9. Lower curve: Maximum vertical velocity vs. Pr at $Ra = 6 \times 10^5$: symbols, numerical results; ———, $U/\mathscr{U} \sim Pr^{-0.22}$ fit. Upper curve: the same but for the horizontal temperature difference: - - - -, $\Delta_h/\Delta \sim 0.6$.

we are aware only of the work of Tilgner (1996) who investigated the parametric effect of Pr. Tilgner (1996), for thermal convection between concentric spheres, has found that the Reynolds number decreases as Pr increases, following different power laws depending on the Pr value. In particular, for $Pr \lesssim 0.5$ he found $Re \sim Pr^{-0.73}$ while for $Pr > 0.5$ the law $Re \sim Pr^{-0.92}$ applied. As already mentioned Tilgner's flow configuration does not allow a direct comparison with our results; however, once again our Re dependence on Pr is in agreement with Tilgner's findings (figure 8*b*). This result can be used to estimate the Pr dependence of the factor A in the relation $U \approx A\mathscr{U}$. In fact, we have $Re \approx Ud/\nu = A\mathscr{U}d/\nu = A(Ra/Pr)^{0.5}$. In the previous section we have shown that A can depend on Pr and, in order to satisfy the results of figure 8(*b*) this must be $A \sim Pr^{-0.22}$ for $Pr \lesssim 0.35$ and $A \sim Pr^{-0.44}$ for $Pr > 0.35$. This is confirmed in figure 9 where a direct evaluation of $U/\mathscr{U}$ is shown and the predicted dependence on Pr is observed.

Concerning the horizontal temperature difference Δ_h we are not aware of any result about its dependence on Pr. We can imagine, however, that as long as thermal plumes do not form Δ_h does not change since it is induced by the large-scale flow which is always present. In contrast, when the plumes begin to detach from the plates Δ_h will decrease for the same reason discussed for figure 6. A confirmation of these ideas comes again from figure 9 where direct calculations of Δ_h performed as in figure 6 are presented. We can see that Δ_h does indeed remain constant for $Pr \lesssim 0.35$ while it starts decreasing when Pr exceeds the value of about 0.4. The former results indicates that, in the low Pr regime where the model of §3.2 is applicable, the coefficient B in the relation $\Delta_h \approx B\Delta$ is a truly numerical factor and its Pr dependence is also ruled out.

We can now reconsider (3.2*b*) at constant Ra which, on account of the Pr dependence of A, yields $Nu \sim Pr^{0.14}$ in agreement with the fit found in figure 1(*b*). Similarly to the previous section, from figure 9 we can calculate the numerical values of A and B that, when plugged into (3.2*b*) together with the value of $Ra = 6 \times 10^5$, give $Nu \approx 7.8Pr^{0.14}$. This law is in quantitative agreement with the fit $Nu \approx 8.5Pr^{0.14}$ given in figure 1(*b*), also confirming that the essential features of the flow dependence on Pr are well represented by the present model.

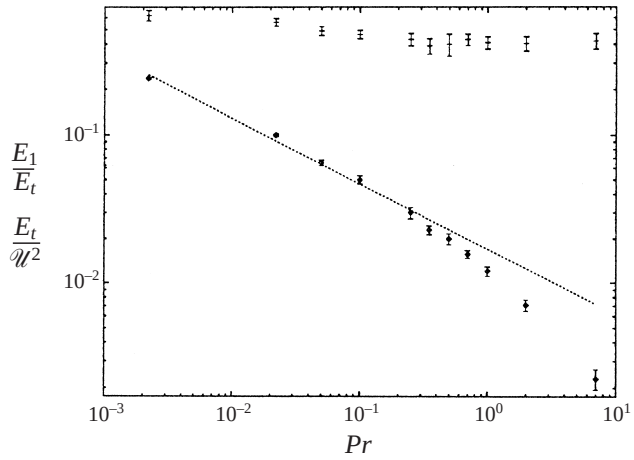

FIGURE 10. Lower curve: total kinetic energy vs. Pr at $Ra = 6 \times 10^5$: ----, $E_t/\mathscr{U}^2 \sim Pr^{-0.44}$ fit. Upper curve: the same but for the percentage of kinetic energy in the $n = 1$ mode (cell strength) vs. Pr at $Ra = 6 \times 10^5$.

It is worth noting that the exponent 0.14 in the Nusselt vs. Prandtl number relation is not a particular value which depends on the Rayleigh number of figure 1(*b*) ($Ra = 6 \times 10^5$) since the same exponent has been found at $Ra = 1.8 \times 10^6$ (using the results and the fits of figure 1(*a*)) and is consistent with the available experimental data (Cioni 1998).

3.5. *Large-scale circulation effects*

Although the effect of the mean circulation on the heat transfer has been studied in several works, a consensus has not yet been reached. For example Shraiman & Siggia (1990) consider the large-scale flow an essential ingredient for the heat transfer, while Belmonte *et al.* (1994) note that, at least in water, the mean flow is too weak to account for the total heat transport. Finally, Ciliberto *et al.* (1996) in their experiment show that complete suppression of the mean flow does not cause variations in the Nusselt number.

From the results of the previous sections we expect that the effect of the large-scale motion depends on the Pr regime of the flow. In fact, as Pr increases the Reynolds number decreases and the large-scale motion weakens. On the other hand, for low Pr thermal plumes are not generated and most of the heat is transferred by the inertial convection of the large cell.

The first argument is addressed in figure 10 where the total kinetic energy and the 'strength' of the large-scale flow are shown. In particular, the lower curve of figure 10 is the total kinetic energy normalized by the squared free-fall velocity, from which it is evident that the larger Pr the smaller the kinetic energy and consequently the weaker the cell. As an aside we note that the slopes of the curve in the two Pr regimes are exactly twice the slopes of figure 9 as should be expected from $E_t \sim U^2$. Further important information about the cell strength is given in the upper curve of figure 10. In fact, when the velocity field is decomposed into azimuthal Fourier modes it is possible to isolate the $n = 1$ energy mode which corresponds to the large-scale recirculation cell.

From figure 10 we can see that as Pr decreases a larger percentage of the total kinetic energy is in the large-scale motion, consistent with the picture that in the low

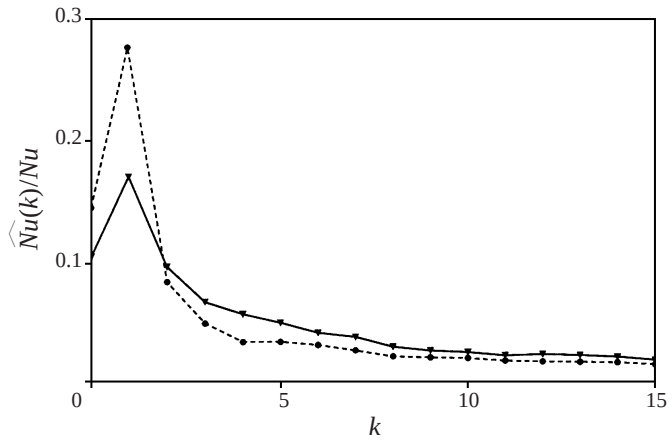

FIGURE 11. Azimuthal non-dimensional Fourier modes $\widehat{Nu}(k)/Nu$ obtained by the Fourier transform in the azimuthal direction of the local Nusselt number $\partial Q/\partial x - (RaPr)^{1/2}(u_x Q)$ averaged over the radial, axial directions and time. – – – –, $Pr = 0.022$ and $Ra = 6 \times 10^5$ ($Re = (Ra/Pr)^{1/2} \simeq 5190$); ———, $Pr = 0.7$ and $Ra = 2 \times 10^7$ ($Re = (Ra/Pr)^{1/2} \simeq 5340$).

Pr regime the large-scale flow is the most important structure. In contrast, in the high Pr regime the energy of the cell seems to be a constant percentage of the total energy even though the cell strength continues to decrease because the total kinetic energy decreases with Pr. The fact that the heat transport due to the large-scale motion is fundamental at low Prandtl number is shown in figure 11 where the azimuthal modes ($\widehat{Nu}(k)$) of the local Nusselt number are shown. It is clear that at low Pr there is an intense peak for $k = 1$ which is the effect of the convective cell while the higher modes decrease rapidly. On the other hand, at $Pr = 0.7$ the peak is less intense and the higher modes become more important since substantial heat transfer is due to small-scale structures (plumes).

If the analysis above is correct we can conjecture that when the large-scale motion is suppressed the Nusselt number has to remain more or less constant if the flow is in the high Pr regime while the Nusselt number has to decrease substantially in the low Pr regime.

In order to suppress the mean flow one possibility is to insert some screens into the cell as in the experiment by Ciliberto *et al.* (1996). However, from the numerical point of view this is extremely complicated and at the moment is beyond our computing capabilities. The easiest way we could think of to suppress the large-scale flow was to perform the simulations imposing axial symmetry. One could argue that in this way the temperature fluctuations could be artificially reduced since the flow is not allowed to have azimuthal gradients. However, should this be true, the effect would be greater for high Pr when the flow can produce tiny localized temperature variations rather than in the low Pr regime where the temperature field is essentially diffusive. On the contrary, when the results are analysed it is only the low Pr case that shows substantial differences from the three-dimensional flow; therefore the axisymmetric approximation can be used for this analysis.

In figure 12, snapshots of the axisymmetric counterparts of the flows of figure 2 are reported and large differences arise. Figure 12(*b*) shows that the mean flow now consists of an array of counter-rotating toroidal structures whose effect on the temperature is to induce a field with the high temperatures ($Q > 0.5$) confined to the

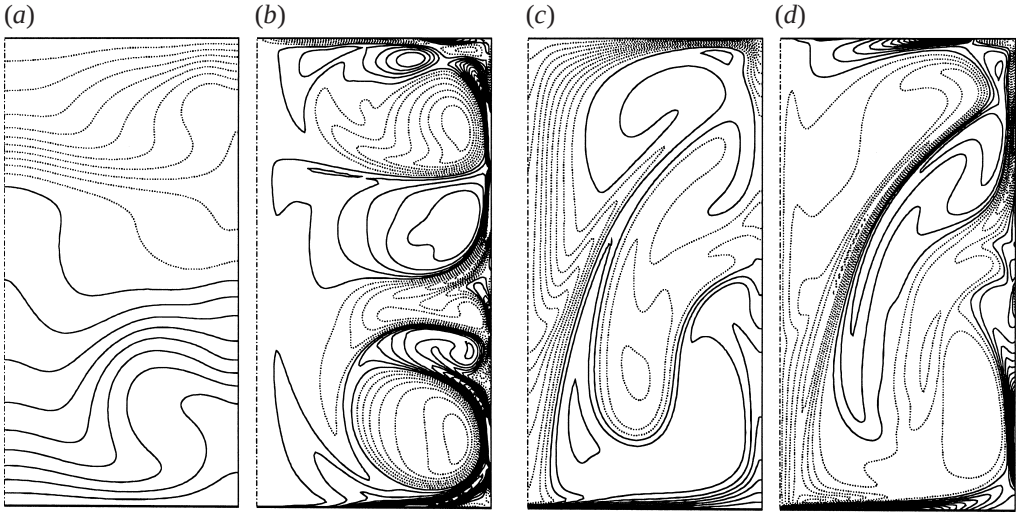

FIGURE 12. Snapshots of vertical cross-sections at $Pr = 0.022$ and $Ra = 10^6$ (a, b) and at $Pr = 0.7$ and $Ra = 2 \times 10^7$ (c, d). Left: temperature contour plots: ———, $0.5 \leqslant Q \leqslant 1$; ·····, $0 \leqslant Q < 0.5$ $(\Delta Q = 0.05)$. Right: azimuthal vorticity: ———, clockwise; ·····, counter clockwise rotation $(\Delta\omega = 2.0)$.

lower half of the domain and vice versa for the upper half. It is clear that in this configuration, where the horizontal temperature differences are zero by definition, the model described in §3.2 is not applicable and a large difference with respect to the Nusselt number of the three-dimensional flow has to be expected. The situation is very different for the simulation at $Pr = 0.7$ where thermal plumes can still form and high-temperature bubbles of fluid can reach the upper plate. This implies that if indeed the thermal plumes are the main mechanism for heat transfer this must be more or less equivalent in this case and in the three-dimensional flow. The calculations of Nusselt number are consistent with the described dynamics. In fact, we have $Nu = 5.1 \pm 0.30$ in the three-dimensional case at $Pr = 0.022$ and $Ra = 10^6$ while it drops to $Nu = 3.22 \pm 0.65$ in the axisymmetric flow. In contrast at $Pr = 0.7$ and $Ra = 2 \times 10^7$ we obtained $Nu = 21.35 \pm 0.31$ in the three-dimensional flow and $Nu = 19.80 \pm 1.95$ for the axisymmetric configuration. The same trend is confirmed by the Reynolds number that at $Pr = 0.022$ decreases about 30% in the axisymmetric case with respect to the three-dimensional case while at $Pr = 0.7$ it remains essentially unchanged. These results confirm that in the low Pr regime the large-scale motion is essential for the heat transport and the model proposed in this paper accounts for this fundamental flow feature. On the other hand for high Pr flows the thermal plumes are responsible for most of the heat transport in which the large-scale motion plays a negligible role. This is in agreement with the scenario proposed by Castaing *et al.* (1989) and with the experiment by Ciliberto *et al.* (1996). Kerr (1996) made similar analyses in a large aspect ratio cell and he also concluded that a recirculation pattern is not necessary to get the $2/7$ exponent at $Pr = 0.7$.

4. Closing remarks

The dynamics of a turbulent convective flow has been analysed for different values of the Prandtl number. The main focus was on the heat transfer with a particular

interest in the different mechanisms occurring for low and high Prandtl numbers. The results of the present numerical simulations, integrated with other numerical and experimental data available in the literature, have shown that there is a value for the Prandtl number ($Pr_t \approx 0.35$) which separates distinct flow regimes. For Prandtl numbers higher than this threshold thermal plumes are generated at the hot and cold horizontal plates and they are able to penetrate the bulk of the flow and to reach the opposite plate. This is the most effective mechanism for heat transfer and a model based on the described features yields $Nu \sim Ra^{2/7}$ (Castaing *et al.* 1989). This value agrees with the results obtained here in the high Pr regime and with the experiments performed in similar conditions. At the same time a large-scale motion is present in the cell that generates a persistent wind sweeping the horizontal plates. This wind induces viscous and thermal boundary layers whose thickness, δ_v and δ_T respectively, depends on the value of the Rayleigh number. For the Rayleigh numbers affordable in the present simulations δ_v and δ_T are of comparable size but both of them decrease with Ra and since δ_T decreases faster than δ_v the inequality $\delta_T \ll \delta_v$ eventually holds for increasing Ra. In agreement with Belmonte *et al.* (1994) and Ciliberto *et al.* (1996) we have found that while the large-scale motion determines the structure of the boundary layers it plays a negligible role in the heat transport because it weakens as the Prandtl number increases. As further confirmation an example has been shown in which the large-scale flow was artificially suppressed by imposing axial symmetry and the Nusselt number remained essentially unchanged with respect to the full three-dimensional case.

When the Prandtl number is below the threshold $Pr_t \approx 0.35$ the flow dynamics are substantially different. In particular the temperature is too diffusive for thermal plumes to be generated and the temperature distribution is determined by the effect of the large-scale motion. This implies that vertical currents of hot and cold fluid are produced on the lateral wall of the cell and the heat transfer process occurs during the horizontal motion of the currents along the thermal boundary layers (figure 2*a*). Also in this case, the large-scale motion induces viscous and thermal boundary layers; however, given the low value of Pr, the condition $\delta_v \ll \delta_T$ applies. The dynamics described have been used to extend and validate a model derived by Jones *et al.* (1976) and reconsidered by Busse & Clever (1981). This model predicted the correct behaviour of the dependence of the Nusselt number on the Rayleigh and Prandtl number at least for the range of parameters investigated. The fact that the predictions of the model are in qualitative and quantitative agreement with the results in the literature confirms that the essential features of the heat transport in low Prandtl number flows are correctly accounted for. Once again an example in which the large-scale motion is artificially suppressed has been shown; in this case, however, the fundamental effect of the mean flow was absent and therefore the heat transfer was drastically reduced.

The simultaneous use of the results of §§3.3 and 3.4 gives the expression for the Nusselt number $Nu \approx 0.27 Pr^{0.14} Ra^{0.25}$, where the numerical prefactor and the exponent 0.14 of Pr come from the results of figures 6, 7 and 9. It is worth noting that these figures were used only to estimate A and B introduced in §3.2 and therefore the proposed law should not be considered purely as a fit to experimental data. This law predicts quite well the Nusselt number even in a range of parameters which was not covered by the present simulations. For example, for sodium the formula gives $Nu \approx 0.124 Ra^{0.25}$ which is not far from the fit $Nu \approx 0.119 Ra^{0.25}$ of figure 1(*a*) while in mercury at $Ra = 10^9$ the above expression yields $Nu \simeq 28.7$ while the experimental value from Cioni *et al.* (1997) is $Nu \simeq 29.5$. We have already mentioned that the

validity of this formula is restricted to the low Pr regime which was found to be $Pr \lesssim 0.35$; of course this value does not fix a sharp transition but rather it indicates a region where the flow smoothly changes from one regime to the other.

We are indebted to S. Cioni for countless suggestions and remarks during the preparation of the work, and for providing several experimental data. We acknowledge S. Ciliberto, J. Sommeria and B. Castaing for several discussions during the data analysis.

The research was partially supported by grants from ASI (Agenzia Spaziale Italiana) and Murst (Ministero dell'Università e della Ricerca Scientifica e Tecnologica).

REFERENCES

Belmonte, A., Tilgner, A. & Libchaber, A. 1994 Temperature and velocity boundary layers in turbulent convection. *Phys. Rev.* E **50**, 269–279.

Busse, F. H. & Clever, R. M. 1981 An asymptotic model of two dimensional convection in the limit of low Prandtl number. *J. Fluid Mech.* **102**, 75–83.

Camussi, R. & Verzicco, R. 1998 Turbulent convection in mercury: scaling laws and spectra. *Phys. Fluids* **10**, 516–527.

Castaing, B., Gunaratne, G., Heslot, F., Kadanoff, L., Libchaber, A., Thomae, S., Wu, X. Z., Zaleski, S. & Zanetti, G. 1989 Scaling of hard thermal turbulence in Rayleigh–Bénard convection. *J. Fluid Mech.* **204**, 1–30.

Chillá, F., Ciliberto, S., Innocenti, C. & Pampaloni, E. 1993 Boundary layer and scaling properties in turbulent thermal convection. *Il Nuovo Cimento* **15**, 1229–1249.

Ciliberto, S., Cioni, S. & Laroche, C. 1996 Large scale flow properties of turbulent thermal convection. *Phys. Rev.* E **54**, 5901–5905.

Cioni, S. 1998 Turbulent natural convection at low Prandtl number. *Proc. 11th Turbulent Shear Flows Conf, 1997, Grenoble.*

Cioni, S., Ciliberto, S. & Sommeria, J. 1997 Strongly turbulent Rayleigh–Bénard convection in mercury: comparison with results at moderate Prandtl number. *J. Fluid Mech.* **335**, 150–181.

Grötzbach, G. 1983 Spatial resolution requirements for direct numerical simulation of the Rayleigh–Bénard convection. *J. Comput. Phys.* **49**, 241–264.

Horanyi, S., Krebs, L. & Müller, U. 1997 Turbulent Rayleigh–Bénard convection in low Prandtl-number fluids. *Intl J. Heat Mass Transfer* (submitted).

Jones, C. A., Moore, D. R. & Weiss, N. O. 1976 Axisymmetric convection in a cylinder. *J. Fluid Mech.* **73**, 353–388.

Kerr, R. M. 1996 Rayleigh number scaling in numerical convection. *J. Fluid Mech.* **310**, 139–179.

Kraichnan, R. 1962 Turbulent thermal convection in arbitrary Prandtl number. *Phys. Fluids* **5**, 1374–1389.

Naert, A., Segawa, T. & Sano, M. 1997 High-Reynolds number thermal turbulence in mercury. *Phys. Rev.* E **56**, 1302–1305.

Rossby, H. T. 1969 A study of Bénard convection with and without rotation. *J. Fluid Mech.* **36**, 309–335.

Shraiman, B. I. & Siggia, E. D. 1990 Heat transport in high Rayleigh–Bénard convection. *Phys. Rev.* A **42**, 3650–3653.

Takeshita, T., Segawa, T., Glazier, J. A. & Sano, M. 1996 Thermal turbulence in mercury. *Phys. Rev. Lett.* **76**, 1465–1468.

Tilgner, A. 1996 High-Rayleigh number convection in spherical shells. *Phys. Rev.* E **53**, 4847–4851.

Verzicco, R. & Camussi, R. 1997 Transitional regimes of low-Prandtl thermal convection in a cylindrical cell. *Phys. Fluids* **9**, 1287–1295.

Verzicco, R. & Orlandi, P. 1996 A finite-difference scheme for three-dimensional incompressible flow in cylindrical coordinates. *J. Comput. Phys.* **123**, 402–413.

Xin, Y.-B., Xia, K.-Q. & Tong, P. 1996 Measured velocity boundary layers in turbulent convection. *Phys. Rev. Lett.* **77**, 1266–1269.